



## Effect of lattice compression on the ${}^7\text{Li}$ recoil energy spectrum following electron capture decay of ${}^7\text{Be}$

A. Ray ,\* P. Das, and A. K. Sikdar *Variable Energy Cyclotron Center 1/AF, Bidhannagar, Kolkata 700064, India*

(Received 9 January 2024; accepted 23 August 2024; published 9 September 2024)

The significant increase in the ( $L/K$ ) ratio of  ${}^7\text{Be}$  implanted in tantalum, compared to that in mercury telluride, has been quantitatively explained by using *ab initio* density functional calculations. The result highlights the effect of lattice compression on the ( $L/K$ ) ratio of  ${}^7\text{Be}$ . Predictions for the ( $L/K$ ) ratio in several untested cases have also been provided. Density functional calculations were employed to understand the notable ( $\approx 6$  eV) downward shift observed in the  $K$  capture to the nuclear ground state ( $K$ -GS) peak in the recoil energy spectrum of  ${}^7\text{Li}$  following the electron capture decay of  ${}^7\text{Be}$  implanted in a small tantalum lattice and the resulting reduced energy difference between the  $K$ -GS and  $L$ -GS peaks. No such anomaly was observed when  ${}^7\text{Be}$  was implanted in mercury telluride. The calculations predict that the chemical shifts of the  ${}^7\text{Li}$   $1s$  state for the implantation of  ${}^7\text{Li}$  in different media are  $\approx (0-2)$  eV. We hypothesize that the observed large downward shift of the  $K$ -GS peak in the  ${}^7\text{Li}$  recoil spectrum might be attributed to the difference of Fermi energies of tantalum and mercury telluride.

DOI: [10.1103/PhysRevC.110.035802](https://doi.org/10.1103/PhysRevC.110.035802)

### I. INTRODUCTION

The current generation of searches for physics beyond the standard model (BSM) delves deeply into the neutrino sector [1–3] with a particular focus on studying the electron capture processes. The approach involves implanting electron capturing nuclei of interest in cryogenic high resolution detectors to measure the corresponding recoil energy spectrum with a high precision. The high precision measurement of the decay energy and spectral shape might enable the identification of any small anomalies of the decay spectrum that could indicate the presence of massive neutrinos or physics beyond the standard model. Recently, Friedrich *et al.* [2] put limits on the existence of sub-MeV sterile neutrinos from the electron capture decay of  ${}^7\text{Be}$ . There are many astrophysical significances of the electron capture decay rate of  ${}^7\text{Be}$  in various astrophysical conditions [4–6]. Additionally, presently ongoing experiments aim to measure the mass of the electron-neutrino from the electron capture decay spectrum of  ${}^{163}\text{Ho}$  [1,3]. To succeed in these endeavors, it is extremely important to understand the effect of the host material on the recoil energy spectrum and decay rate following the electron capture process.

Voytas *et al.* [7] and Fretwell *et al.* [6] measured  ${}^7\text{Li}$  recoil energy spectrum following the decay of implanted  ${}^7\text{Be}$  in large mercury telluride (HgTe) and small tantalum (Ta) lattices. Voytas *et al.* [7] implanted  ${}^7\text{Be}$  in the samples of mercury telluride mounted on a cryogenic microcalorimeter and measured  ${}^7\text{Li}$  recoil energy spectrum from the observed temperature rise. Recently, Fretwell *et al.* [6] implanted  ${}^7\text{Be}$  in a Ta-based superconducting tunnel junction and measured the  ${}^7\text{Li}$  recoil energy spectrum from the tunnel current. In the electron capture (EC) process of  ${}^7\text{Be}$ , an electron could be

captured either from the  $1s$  orbital ( $K$  capture) or  $2s$  orbital ( $L$  capture). In the  ${}^7\text{Li}$  recoil energy spectrum, the observed  $L$ -GS peak originates from the  $L$  capture to the nuclear ground state of  ${}^7\text{Li}$ , primarily exhibiting the  ${}^7\text{Li}$  recoil energy due to the emission of an 862.89 keV electron-neutrino [8]. The observed  $K$ -GS peak is the sum of the  ${}^7\text{Li}$  recoil energy and the energy deposited by the Auger electron(s) produced in the course of filling up the  $K$  vacancy. In addition, smaller  $K$ -ES and  $L$ -ES peaks are seen, because both the  $K$  and  $L$  electron capture process have a 10.4% branching ratio of populating the first excited state (477.6 keV) of  ${}^7\text{Li}$ , thus emitting an electron-neutrino of energy 385.29 eV and a  $\gamma$ -ray photon of energy 477.6 eV. Samanta *et al.* [9] performed density functional calculations to understand the widths of  $K$ -GS and  $L$ -GS peaks for  ${}^7\text{Be}$  implanted in the tantalum lattice and found that the presence of lithium in different lattice sites and in the vicinity of various impurities contribute significantly to the broadening of the peaks, although they could not account for the full extent of the observed broadening. Apart from the challenges of understanding the widths of the  $K$ -GS and  $L$ -GS peaks, there were other unexplained observations, such as the significantly higher ( $L/K$ ) ratio for  ${}^7\text{Be}$  implanted in tantalum, compared to mercury telluride, and the downward shift of the  $K$ -GS peak in the  ${}^7\text{Li}$  recoil energy spectrum following the decay of  ${}^7\text{Be}$  in tantalum [6,7]. The goal of this paper is to understand these observations.

Fretwell *et al.* [6] measured the  ${}^7\text{Li}$  recoil energy spectrum following the decay of  ${}^7\text{Be}$  in tantalum and found that the ( $\frac{L}{K}$ ) ratio of  ${}^7\text{Be}$  in tantalum is  $0.070 \pm 0.007$ . The only previous measurement of this ratio obtained from the decay of  ${}^7\text{Be}$  in mercury telluride was  $0.040 \pm 0.006$ . Earlier theoretical calculations [10] suggested a change in this ratio from the predications for a free  ${}^7\text{Be}$  atom in a vacuum with two full  $2s$  electrons due to medium effect. However, these calculations failed to explain the higher value observed in the small tanta-

\*Contact author: [amlanray2016@gmail.com](mailto:amlanray2016@gmail.com)

TABLE I. Centroids of  $K$ -GS and  $L$ -GS peaks and their differences in the  ${}^7\text{Li}$  recoil spectra.

Centroid of $K$ -GS ( ${}^7\text{Be}$ decaying in HgTe) [7]	Centroid of $L$ -GS ( ${}^7\text{Be}$ decaying in HgTe) [7]	Centroid of $K$ -GS ( ${}^7\text{Be}$ decaying in Ta) [6]	Centroid of $L$ -GS ( ${}^7\text{Be}$ decaying in Ta) [6]	Energy difference between $K$ -GS centroids for ${}^7\text{Be}$ decaying in HgTe versus Ta ( $\Delta E_{K-GS}$ )
$(112.6 \pm 0.2)$ eV	$(57.5 \pm 0.5)$ eV	$(106.4 \pm 0.2)$ eV	$(58.3 \pm 0.5)$ eV	$(6.2 \pm 0.3)$ eV

lum lattice. These calculations [10] placed  ${}^7\text{Be}$  in  $(1 \times 1 \times 1)$  lattices and performed density functional calculations without considering the distortions of the lattices due to the insertion of  ${}^7\text{Be}$  atoms. Some of the  $2s$  electrons of  ${}^7\text{Be}$  became hybridized with the atomic states of the host lattice, and the remaining number of orbital  $2s$  electrons ( $n_{2s}$ ) was calculated. A correction factor ( $\frac{n_{2s}}{2}$ ) was then applied to the theoretical predictions [11,12] of  $(\frac{L}{K})_{\text{vacuum}}$  for a free  ${}^7\text{Be}$  atom in a vacuum with two full  $2s$  electrons to account for the medium effect. Therefore, these calculations essentially considered the effect of electron affinity of the host medium without taking into account the effect of lattice pressure on the increase of  $2s$  electron density at the  ${}^7\text{Be}$  nucleus. As a result, these calculations [10] should be considered qualitative, and more detailed calculations that compute the  $1s$  and  $2s$  electron densities at the  ${}^7\text{Be}$  nucleus, including all lattice effects, are required.

To elucidate the problem of  $K$ -GS shifts, we determined the centroids of the  $L$ -GS and  $K$ -GS peaks from the  ${}^7\text{Li}$  recoil energy spectrum following the decay of  ${}^7\text{Be}$  implanted in mercury telluride (HgTe) [7] and tantalum (Ta) [6] and tabulate the results in Table I. To account for the different peak shapes, the centroids of the  $K$ -GS and  $L$ -GS peaks have been calculated using weighted arithmetic averages over the fitted peak shapes as shown in Refs. [6] and [7]. The fitted peak shape takes care of the overlap between the neighboring peaks and the characteristics of the shape of the peak. The statistical error is very small. However, the centroid position of the peak could change by  $\approx 0.5$  eV (for the  $L$ -GS peaks) and  $\approx 0.2$  eV (for the  $K$ -GS peaks) depending on the regions of the peak over which arithmetic averaging was performed. These values have been taken as the uncertainties of the centroid position.

From Table I, we find that the centroid of  $L$ -GS peak remain essentially unchanged within the uncertainties irrespective of whether  ${}^7\text{Be}$  was implanted in HgTe or Ta. To probe if there is any significant nonlinearity in the energy calibration of  ${}^7\text{Li}$  recoil energy spectrum, we determined the energy difference between the centroids of the  $K$ -GS and  $K$ -ES (excited state) peaks and also between  $L$ -GS and  $L$ -ES peaks. These differences are about equal ( $\approx 28$  eV) both from the spectra of Refs. [6] and [7], in agreement with the expected difference. We conclude that the nonlinearity and uncertainty in the energy calibration are not significantly more than 1 eV. On the other hand, the centroid of  $K$ -GS peak shifted down by  $\Delta E_{K-GS} = (6.2 \pm 0.3)$  eV when  ${}^7\text{Be}$  was implanted in Ta compared to implantation in HgTe and the same is true for the  $K$ -ES peak. We apply *ab initio* density functional calculations to understand these problems.

It is important to first verify whether our calculations could reproduce the chemical shift seen in x-ray absorption spectroscopy. We apply *ab initio* density functional WIEN2K code [13] to calculate the measured chemical shift [14] in oxygen

$K$  x-ray absorption spectra of  $\text{Sr}_2\text{CoO}_3\text{Cl}$  versus  $\text{EuCoO}_3$  lattices before attempting to understand the origin of the downward shift of  $K$ -GS peak when  ${}^7\text{Be}$  decays in Ta lattice.

## II. COMPUTATIONAL DETAILS

In the  ${}^7\text{Be}$  decay experiments,  ${}^7\text{Be}$  and subsequently its daughter  ${}^7\text{Li}$  were implanted in tantalum and mercury telluride lattices randomly with an average concentration of one  ${}^7\text{Be}$  in  $10^9$ – $10^{11}$  host lattices. We approximate the situation by constructing supercells in the context of density functional WIEN2K code. We combine 8 adjacent lattices ( $2 \times 2 \times 2$ ), where each tantalum lattice is a body centered cubic lattice of lattice constant = 3.306 Å at room temperature [15]. Similarly for the implantations of  ${}^7\text{Be}$  or  ${}^7\text{Li}$  in mercury telluride, supercells were constructed by combining eight adjacent lattices ( $2 \times 2 \times 2$ ) of mercury telluride, where each lattice of mercury telluride comprises two face-centered cubic lattices of mercury and tellurium displaced from each other by one quarter of a body diagonal and the lattice parameter of a mercury telluride lattice is 6.462 Å at room temperature [16]. A  ${}^7\text{Be}$  or  ${}^7\text{Li}$  atom was kept at the octahedral site of each supercell and the periodic boundary condition was applied. Point nuclei and relativistic Dirac wave functions were used for the electronic calculations. The calculations are based on the full potential (linearized) augmented plane-wave and local orbital methods. The generalized gradient approximation with the parametrization of Perdew, Burke and Ernzerhof (PBE) was used for the exchange correlation function [13]. The total energy convergence was better than 1 meV/atom and the charge convergence in the muffin-tin sphere was on the order of  $10^{-3}e/(\text{Bohr unit})^3$ . In the case of implantations of  ${}^7\text{Be}$  or  ${}^7\text{Li}$  in the interstitial spaces, the distortions of the lattices are considered by shifting the atoms of the lattices to minimize forces on them to the order of 1 mRy/Bohr unit along with minimizing the total energy.  $1s$  electrons of  ${}^7\text{Be}$  were considered as core electrons and its  $2s$  electrons were considered as valence electrons in the calculations. The code calculates core and valence electron densities at different radial distances from the point  ${}^7\text{Be}$  nucleus, considering the effect of electronic screening. The ratio of  $2s$  to  $1s$  electron densities at different radial distances close to the nucleus remain about the same. We take this ratio at the radial distance of 2.6 fermi from the point  ${}^7\text{Be}$  nucleus. Although in the actual experiments, the concentration of  ${}^7\text{Be}$  or  ${}^7\text{Li}$  in the lattices was much lower compared to that in our  $(2 \times 2 \times 2)$  supercell construction with one  ${}^7\text{Be}$  or  ${}^7\text{Li}$  atom in the octahedral position of each supercell, the results do not change significantly for  $(3 \times 3 \times 3)$  supercell construction and so we have performed our calculations using  $(2 \times 2 \times 2)$  supercell construction. The insertion of  ${}^7\text{Li}$  in the tetrahedral position

of the tantalum lattice did not give a stable solution and so we only considered implantations in the octahedral sites of the lattice. To calculate the measured chemical shifts found in oxygen  $K$  x-ray absorption spectra of  $\text{Sr}_2\text{CoO}_3\text{Cl}$  versus  $\text{EuCoO}_3$ , we performed density functional WIEN2K code [13] calculations for  $\text{Sr}_2\text{CoO}_3\text{Cl}$  and  $\text{EuCoO}_3$  lattices. The lattice structures and space groups of  $\text{EuCoO}_3$  and  $\text{Sr}_2\text{CoO}_3\text{Cl}$  lattices have been obtained from Refs. [17,18]. WIEN2K code [13] provides the Fermi energy ( $E_{\text{Fermi}}$ ) of the medium and the eigenvalues of the atomic electronic states with respect to the average Coulomb potential in the interstitial regions of the lattice. This allows us to calculate the eigenvalues of the atomic electronic states with respect to the Fermi energy of the lattice.

### III. RESULTS AND DISCUSSIONS

#### A. Increased $L/K$ ratio for $^{7}\text{Be}$ in Ta medium

In the case of a free  $^{7}\text{Be}$  atom in a vacuum with two full  $2s$  electrons, the calculated ratio of  $2s$  to  $1s$  electron density at the  $^{7}\text{Be}$  nucleus is 0.0331 [11]. When  $^{7}\text{Be}$  is placed in a lattice, it loses some of its  $2s$  electrons, which become hybridized with the atomic states of the lattice atoms. As a result,  $2s$  electron density at the  $^{7}\text{Be}$  nucleus decreases. On the other hand, lattice compression on the orbital  $2s$  electrons pushes them towards the nucleus, increasing  $2s$  electron density at the  $^{7}\text{Be}$  nucleus and slightly reducing  $1s$  electron density at the nucleus due to the screening effect of the  $2s$  electrons [19]. Qualitatively, the  $2s$  electron density at the  $^{7}\text{Be}$  nucleus is expected to increase significantly when  $^{7}\text{Be}$  is implanted in the small tantalum lattice compared to the large mercury telluride lattice.

*Ab initio* density functional calculations (WIEN2K code) [13] naturally include all these effects. We find that for  $^{7}\text{Be}$  implanted in the octahedral site of a tantalum superlattice ( $2 \times 2 \times 2$ ), the ratio of  $2s$  to  $1s$  electron densities at the  $^{7}\text{Be}$  nucleus is  $\frac{\rho(r=2.6 \text{ fm})_{2s}}{\rho(r=2.6 \text{ fm})_{1s}} = 0.037$ . The corresponding ratio for  $^{7}\text{Be}$  implanted in the octahedral site of mercury telluride superlattice ( $2 \times 2 \times 2$ ) is  $\frac{\rho(r=2.6 \text{ fm})_{2s}}{\rho(r=2.6 \text{ fm})_{1s}} = 0.025$ , where  $\rho(r=2.6 \text{ fm})_{2s}$  and  $\rho(r=2.6 \text{ fm})_{1s}$  are the  $2s$  and  $1s$  electron densities of  $^{7}\text{Be}$  at a radial distance of  $r = 2.6 \text{ fm}$  from the point  $^{7}\text{Be}$  nucleus. The ratio of electron densities does not change significantly for calculations at somewhat different distances from the center of the nucleus. The  $(L/K)$  ratio for  $^{7}\text{Be}$  is given by [12,20]

$$\frac{L}{K} = \left( \frac{\rho_{2s}}{\rho_{1s}} \right) \times \left( \frac{q_{2s}}{q_{1s}} \right)^2 X^{L/K},$$

where  $\rho_{1s}$  and  $\rho_{2s}$  are the electron densities at the  $^{7}\text{Be}$  nucleus,  $q_{2s}$  and  $q_{1s}$  are the neutrino energies for the capture of  $2s$  and  $1s$  electrons of  $^{7}\text{Be}$ , and  $X^{L/K}$  is the corresponding correction factor due to the overlap and exchange effects [12,20]. The  $(L/K)$  ratio for  $^{7}\text{Be}$  was measured from the  $^{7}\text{Li}$  recoil energy spectrum by taking the ratio of the areas under the  $L$ -GS and  $K$ -GS peaks. We calculate  $(L/K)$  ratios by comparing them with the experimentally measured  $(L/K)$  ratio of  $^{7}\text{Be}$  decaying in mercury telluride ( $\text{HgTe}$ ) [7], rather than with the theoretical predictions [12] of  $\left(\frac{L}{K}\right)_{\text{vacuum}}$  for a free  $^{7}\text{Be}$  atom in a vacuum, to properly account for the  $X^{L/K}$  factor. Based on

our density functional calculations (WIEN2K), the  $(L/K)$  ratio for  $^{7}\text{Be}$  implanted in mercury telluride is given by [12,20]

$$\begin{aligned} \left( \frac{L}{K} \right)_{\text{HgTe}} &= \left( \frac{\rho(r=2.6 \text{ fm})_{2s}}{\rho(r=2.6 \text{ fm})_{1s}} \right)_{\text{HgTe}} \times \left( \frac{q_{2s}}{q_{1s}} \right)^2 X^{L/K} \\ &\approx 0.025 \times X^{L/K}. \end{aligned}$$

Similarly the  $(L/K)$  ratio for  $^{7}\text{Be}$  implanted in tantalum is given by

$$\begin{aligned} \left( \frac{L}{K} \right)_{\text{Ta}} &= \left( \frac{\rho(r=2.6 \text{ fm})_{2s}}{\rho(r=2.6 \text{ fm})_{1s}} \right)_{\text{Ta}} \times \left( \frac{q_{2s}}{q_{1s}} \right)^2 X^{L/K} \\ &\approx 0.037 \times X^{L/K}. \end{aligned}$$

The percentage change of neutrino energies for the decay of  $^{7}\text{Be}$  in mercury telluride or tantalum is negligible, because the  $Q$  value of the electron capture process is about 862 keV, whereas the  $1s$  bound state energy of  $^{7}\text{Li}$  is  $\approx -51.1 \text{ eV}$  and hence the quantity  $\left(\frac{q_{2s}}{q_{1s}}\right)$  has been kept unchanged for the implantations of  $^{7}\text{Be}$  in  $\text{HgTe}$  versus Ta. Moreover, we can take  $q_{1s} \approx q_{2s}$ . We have kept correction factor  $X^{L/K}$  the same in the two situations, because of its weak dependence on the atomic potential [12]. Then our calculated  $(L/K)$  ratios in the two cases is given by

$$\frac{\left(\frac{L}{K}\right)_{\text{Ta}}}{\left(\frac{L}{K}\right)_{\text{HgTe}}} = \frac{0.037}{0.025} = 1.48,$$

where as the corresponding experimental value as obtained from Refs. [6] and [7] is  $\frac{0.070 \pm 0.007}{0.040 \pm 0.006} = 1.75 \pm 0.32$ , in agreement with the calculations. Comparing with the value of  $\left(\frac{L}{K}\right)_{\text{HgTe}} = 0.040 \pm 0.006$ , as obtained from Ref. [7], and tak-

ing our theoretically calculated value of  $\left(\frac{L}{K}\right)_{\text{HgTe}} = 1.48$ , we get  $\left(\frac{L}{K}\right)_{\text{Ta}} = 0.059 \pm 0.009$ , in agreement with the corresponding measured  $(L/K)$  ratio of  $0.070 \pm 0.007$  [6]. Our results indicate that the lattice compression effect caused by the small tantalum lattice is more significant than the loss of  $2s$  electrons of  $^{7}\text{Be}$  in the tantalum medium. Consequently, the final outcome is an increase in the  $2s$  electron density at the  $^{7}\text{Be}$  nucleus, when  $^{7}\text{Be}$  is implanted in tantalum, compared to when it is implanted in mercury telluride medium.

Similarly, by comparing with the measured  $\left(\frac{L}{K}\right)_{\text{HgTe}}$ , we have determined the  $(L/K)$  ratios of  $^{7}\text{Be}$  implanted in several other media and updated many of our previous results [10], which can now be tested. All these results are presented in Table II. In all these cases, we performed calculations by implanting  $^{7}\text{Be}$  in the octahedral positions of the ( $2 \times 2 \times 2$ ) superlattices. We find from Table II that  $\left(\frac{L}{K}\right)_{\text{Pd}}$  is higher than  $\left(\frac{L}{K}\right)_{\text{Pt}}$ , because of the higher lattice pressure exerted by the smaller Pd lattice on  $^{7}\text{Be}$  atom. The electron affinities of Pt and Pd are similar [15]. On the other hand,  $\left(\frac{L}{K}\right)_{\text{Au}} \approx \left(\frac{L}{K}\right)_{\text{Al}}$ . The loss of  $2s$  electrons of  $^{7}\text{Be}$  implanted in gold due to its higher electron affinity compared to that of aluminum [15] seems to be compensated by the higher lattice pressure exerted by the larger gold atoms on the  $2s$  electrons. We studied the variations in the  $\left(\frac{L}{K}\right)$  ratio for the implantation of  $^{7}\text{Be}$  in the octahedral and tetrahedral positions of an Au lattice. By

TABLE II.  $L/K$  ratios of  ${}^7\text{Be}$  implanted in different media. Subscripts denote the media.

Quantities	Calculated	Experimental
$(L/K)_{\text{Ta}}/(L/K)_{\text{HgTe}}$	1.48	$1.75 \pm 0.32$
$(L/K)_{\text{Ta}}$	$0.059 \pm 0.009$	$0.070 \pm 0.007$
$(L/K)_{\text{Pd}}$	$0.049 \pm 0.007$	No data available
$(L/K)_{\text{Pb}}$	$0.038 \pm 0.006$	No data available
$(L/K)_{\text{Au}}$	$0.043 \pm 0.007$	No data available
$(L/K)_{\text{Al}}$	$0.043 \pm 0.006$	No data available
$(L/K)_{\text{LiF}}$	$0.069 \pm 0.010$	No data available

minimizing the forces on the lattice atoms to account for lattice distortion, we found that the average ( $\frac{L}{K}$ ) ratio, weighted over the octahedral and tetrahedral positions, changed by only 5%. Given our other uncertainties, we have neglected these corrections and considered the results for the implantation of  ${}^7\text{Be}$  in the octahedral position only. Therefore, the current *ab initio* calculations performed using the WIEN2K code [13] represent a significant advancement compared to our previous calculations [10], which were based only on the loss of orbital  $2s$  electrons of  ${}^7\text{Be}$  atom within the lattice environment.

From a comparison of our calculated ( $\frac{L}{K}$ )<sub>Ta</sub> with the experimental result, we find that WIEN2K code might underpredict this ratio by  $\approx 10\%$ , implying a similar underprediction of  $2s$  electron density at  ${}^7\text{Be}$  nucleus under lattice compression in a small lattice. This could result in an uncertainty of  $\approx 0.5\%$  in the calculated total electron density at the  ${}^7\text{Be}$  nucleus under lattice compression. Therefore, the predictions for the small increase ( $\leq 1\%$ ) of  ${}^7\text{Be}$  decay rate under lattice compression using the WIEN2K code [13] should be viewed as qualitative. It is not surprising that earlier estimates [19] of the increase in the  ${}^7\text{Be}$  decay rate under lattice compression underestimated the experimental results.

### B. Calculation of chemical shifts

The oxygen  $K$ -absorption peaks were observed in the x-ray absorption spectroscopy of  $\text{Sr}_2\text{CoO}_3\text{Cl}$  and  $\text{EuCoO}_3$  lattices at incident photon energies of 528.8 and 529.8 eV respectively [14]. Consequently, the chemical shift of the oxygen  $K$ -absorption peak is approximately 1 eV between  $\text{Sr}_2\text{CoO}_3\text{Cl}$  and  $\text{EuCoO}_3$  lattices. In oxygen  $K$  x-ray absorption spectroscopy, a peak in the spectrum arises when the incident photon elevates a bound  $1s$  electron of oxygen to the half-filled Fermi level of the lattice. This indicates that the energy of the incident photon matches the energy required to excite the  $1s$  electron of oxygen to the Fermi energy of the lattice. Thus, the chemical shift of the oxygen  $K$  x-ray absorption peak in the  $\text{EuCoO}_3$  lattice relative to the  $\text{Sr}_2\text{CoO}_3\text{Cl}$  lattice is given by

$$\Delta E(1s)_{\text{oxygen}} = E(1s)_{\text{oxygen}_{\text{Sr}_2\text{CoO}_3\text{Cl}}} - E(1s)_{\text{oxygen}_{\text{EuCoO}_3}},$$

where  $E(1s)_{\text{oxygen}_{\text{Sr}_2\text{CoO}_3\text{Cl}}}$  and  $E(1s)_{\text{oxygen}_{\text{EuCoO}_3}}$  denote the energies of oxygen  $1s$  state relative to the respective Fermi energy of  $\text{Sr}_2\text{CoO}_3\text{Cl}$  and  $\text{EuCoO}_3$  lattices. Both  $E(1s)_{\text{oxygen}_{\text{Sr}_2\text{CoO}_3\text{Cl}}}$  and  $E(1s)_{\text{oxygen}_{\text{EuCoO}_3}}$  are negative quantities. Calculations using WIEN2K [13] suggest

$\Delta E(1s)_{\text{oxygen}} = 0.8$  eV, indicating that the oxygen  $K$  x-ray absorption peak of the  $\text{EuCoO}_3$  lattice is expected to appear at an incident photon energy 0.8 eV higher than that of the  $\text{Sr}_2\text{CoO}_3\text{Cl}$  lattice. This is in reasonable agreement with the approximately 1 eV shift observed experimentally in the incident photon energy.

The binding energy of the  $1s$  state of a lithium atom in lithium metal relative to its Fermi energy, measured as  $(54.75 \pm 0.02)$  eV [21], is generally regarded as the reference value for the binding energy of Li  $1s$  state. The binding energies of  $1s$  state of lithium atom implanted in different media can be measured by electron energy loss spectroscopy (EELS), allowing the determination of chemical shifts relative to the literature reference value [21]. Let the chemical shift of the lithium  $1s$  state for a lithium atom implanted in a medium, relative to the reference value given for lithium metal be denoted by  $\Delta E(1s)_{\text{Li}}$ . Then  $\Delta E(1s)_{\text{Li}}$  is given by the formula

$$\Delta E(1s)_{\text{Li}} = E(1s)_{\text{Li}_{\text{metal}}} - E(1s)_{\text{Li}_{\text{medium}}},$$

where  $E(1s)_{\text{Li}_{\text{metal}}}$  represents the energy of the  $1s$  state of a lithium atom in lithium metal relative to its Fermi energy, and  $E(1s)_{\text{Li}_{\text{medium}}}$  denotes the energy of the  $1s$  state of implanted lithium atom in a medium relative to the Fermi energy of that medium. Both  $E(1s)_{\text{Li}_{\text{metal}}}$  and  $E(1s)_{\text{Li}_{\text{medium}}}$  are negative quantities.

Using the WIEN2K code [13], we calculated the chemical shifts of lithium atoms implanted in various media relative to the reference literature value and summarized them in Table III. All calculations were performed by inserting a lithium atom in the octahedral site of a  $(2 \times 2 \times 2)$  superlattice and applying periodic boundary conditions. The lattice parameters were taken from Ref. [15]. The calculations predict that the onset energy of  $1s$  state of lithium implanted in Ta, as observed in the EELS spectrum, will be 1.3 eV higher than the reference value measured for lithium in its metallic form. However, for lithium atoms implanted in Au, Al, and Pd, the onset energies are predicted to be about 1–1.5 eV lower than the reference value.

In the next section, we apply this method to calculate the shift of  ${}^7\text{Li}$   $K$ -GS peak in the  ${}^7\text{Li}$  recoil energy spectrum.

### C. Calculation of the shift of ${}^7\text{Li}$ $K$ -GS peak

In the  ${}^7\text{Li}$  recoil energy spectrum following the electron capture decay of  ${}^7\text{Be}$ ,  $L$ -GS peak primarily results from the recoil of the emitted 862.89 keV electron-neutrino, as a  $2s$  electron is captured by  ${}^7\text{Be}$ . The expected recoil energy of  ${}^7\text{Li}$  would be approximately 56.8 eV [2], indicating the position of the centroid of the  $L$ -GS peak. From Table I, we find that the centroids of  $L$ -GS peaks following the electron capture decay of  ${}^7\text{Be}$  implanted in Ta and HgTe [6,7], are in reasonable agreement with this expectation.

On the other hand, in the case of  $1s$  electron capture by  ${}^7\text{Be}$  implanted in a lattice, as the hole in the  $1s$  state of  ${}^7\text{Li}$  is filled, Auger electron(s) are emitted with the kinetic energies much higher than the Fermi energy of the host lattice. These electrons relax to the respective Fermi energy of the host lattice, depositing energy into the lattice. The chemical shift of the  $1s$  state of Li atom implanted in mercury telluride (HgTe)



TABLE III. Calculated and measured chemical shifts in different media.

Shift	Calculated chemical shift	Experimental value
Chemical shift of oxygen $1s$ line between the $\text{EuCoO}_3$ and $\text{Sr}_2\text{CoO}_3\text{Cl}$ lattices	0.8 eV	$\approx 1$ eV
Chemical shift of lithium $1s$ line for lithium atoms implanted in Ta, relative to reference lithium metal	1.3 eV	No data available
Chemical shift of lithium $1s$ line for lithium atoms implanted in HgTe, relative to reference lithium metal	0.5 eV	No data available
Chemical shift of lithium $1s$ line for lithium atoms implanted in Au, relative to reference lithium metal	-0.9 eV	No data available
Chemical shift of lithium $1s$ line for lithium atoms implanted in Al, relative to reference lithium metal	-0.7 eV	No data available
Chemical shift of lithium $1s$ line for lithium atoms implanted in Pb, relative to reference lithium metal	-0.01 eV	No data available
Chemical shift of lithium $1s$ line for lithium atoms implanted in Pd, relative to reference lithium metal	-1.7 eV	No data available
Chemical shift of $^7\text{Li}$ $1s$ line for $^7\text{Li}$ implanted in HgTe, relative to implantation in Ta	-0.8 eV	No data available

relative to implantation in tantalum (Ta) is given by

$$\Delta E(1s)_{\text{Li}} = E(1s)_{\text{Li-Ta}} - E(1s)_{\text{Li-HgTe}} \approx -0.8 \text{ eV}.$$

This result suggests that the binding energy of  $1s$  state of an implanted Li atom in Ta, relative to the Fermi energy of Ta, is 0.8 eV higher than the corresponding binding energy of a Li atom implanted in HgTe. Consequently, based on the chemical shift calculation, the  $K$ -GS peak of  $^7\text{Li}$  in the recoil energy spectrum is predicted to occur at 0.8 eV higher energy when  $^7\text{Li}$  is implanted in Ta compared to when it is implanted in HgTe. However, as shown in Table I, the  $^7\text{Li}$   $K$ -GS peak actually appears 6.2 eV lower in energy when  $^7\text{Li}$  is implanted in Ta compared to when implanted in HgTe. Therefore, the calculated chemical shift predicts the opposite effect. In this context, it is important to examine the uncertainties in the calculated chemical shifts.

The uncertainties in estimating  $1s$  state energies of lithium atom implanted in different media, relative to the Fermi energy of the corresponding host lattices, can arise from several factors. These factors include structural relaxation of the lattice following the implantation of lithium atoms, the choice of exchange-correlation functional, basis states used, and the size of the supercell employed in the calculations. For our computations, we used the standard Perdew, Burke and Ernzerhof parametrization for the exchange correlation functional and the WIEN2K basis states [13]. The  $(2 \times 2 \times 2)$  supercells used in our calculations, appeared to be adequate for our purposes, and the calculated chemical shifts are in reasonable agreement with the available data. We believe that the largest source of uncertainty is the structural relaxation of the lattice following lithium implantation. The relaxation has a direct influence on the local atomic positions and the potential experienced by the implanted lithium atom, which is critical in determining the  $1s$  state energy of the implanted lithium atom, relative to the Fermi energy of the host lattice.

To provide a conservative estimate of the uncertainty, we compared the  $1s$  state energies of implanted lithium atom (relative to the Fermi energy of the host lattice) before and after the structural relaxation of the lattice. The percentage

variation in the  $1s$  state energy of Li atom (before and after lattice relaxation) has been found to be very small (at most  $\approx 1\%$ ). However, this small variation can result in a significantly larger percentage variation in the chemical shift due to the small absolute magnitude of the shifts. For example, the chemical shift (0.8 eV) of oxygen  $K$ -absorption peaks between  $\text{EuCoO}_3$  and  $\text{Sr}_2\text{CoO}_3\text{Cl}$  lattices shows a percentage variation of 11%. In contrast, the percentage variation in the chemical shift of the  $1s$  state energy of Li atoms implanted in Ta compared to lithium metal is only 1%, while for Li implanted in HgTe relative to lithium metal is 3.6%. Variations in the chemical shifts of the  $1s$  line of Li implanted in Pd, Au, and Al relative to lithium metal are 42%, 58%, and 100% respectively. This variation significantly exceeds 100% for the  $1s$  line of Li implanted in Pb relative to lithium metal due to its very small absolute value. To estimate the shift of the  $^7\text{Li}$   $K$ -GS peak in HgTe relative to Ta, we calculated the chemical shift (-0.8 eV) of the  $1s$  state energy of lithium implanted in HgTe relative to Ta. The variation of this chemical shift is only 2.8%. We have not shown these uncertainties in Table III, as they are likely to be gross overestimates and do not account for other potential uncertainties.

Since the Auger electrons relax to the Fermi energy of the host medium, we hypothesize that the difference of Fermi energies of Ta and HgTe should be taken into account. Therefore, the difference  $[\Delta E_{K-GS}]$  between the energies deposited by the Auger electrons in mercury telluride and tantalum lattices, on top of the recoil energy of  $^7\text{Li}$  ( $L$ -GS energy), is given by

$$\begin{aligned} \Delta E_{K-GS} &= E(1s)_{\text{Li-Ta}} - E(1s)_{\text{Li-HgTe}} + \Delta E_{\text{Fermi}} \\ &\approx -0.8 \text{ eV} + \Delta E_{\text{Fermi}}, \end{aligned} \quad (1)$$

where  $\Delta E_{\text{Fermi}}$  represents the difference between the Fermi energies of tantalum and mercury telluride. We conjecture that the difference between the Fermi energies of tantalum and mercury telluride ( $\Delta E_{\text{Fermi}}$ ) could be responsible for the observed shift of the  $K$ -GS peak. The Fermi level in

tantalum is located in the conduction band, while in mercury telluride, it is in the valence band, implying a lower Fermi energy for mercury telluride compared to tantalum. Both the WIEN2K [13] and TB-LMTO calculations [22] indicate that the Fermi level of tantalum is about 7 eV higher than its average interstitial Coulomb potential, whereas the Fermi level of mercury telluride is very close to its average interstitial Coulomb potential. Considering that the kinetic energy of the emitted Auger electron is also with respect to the average interstitial Coulomb potential (the common reference point in the calculations), it will deposit almost its full energy in mercury telluride and less energy in tantalum by relaxing to their respective Fermi energies. By taking the difference of Fermi energies,  $\Delta E_{\text{Fermi}} \approx 7$  eV between tantalum and mercury telluride in the context of these calculations, we obtain from Eq. (1),  $\Delta E_{K-GS} \approx 6$  eV, which is in good agreement with the observed difference of  $(6.2 \pm 0.3)$  eV. Given the calculated small chemical shift ( $\approx 0.5$  eV) of the  ${}^7\text{Li}$   $1s$  line in HgTe compared to lithium metal (as shown in Table III), and the fact that the Fermi level of HgTe is very close to the average interstitial Coulomb potential, it is expected that the energy difference between the centroids of the  $K$ -GS and  $L$ -GS peaks [ $(55.1 \pm 0.5)$  eV] in the recoil energy spectrum of  ${}^7\text{Li}$  following the electron capture decay of  ${}^7\text{Be}$  implanted in HgTe, will be consistent with the experimentally measured binding energy [ $(54.75 \pm 0.02)$  eV] of the  $1s$  state of a Li atom in lithium metal relative to the Fermi energy of the medium [21]. However, for the electron capture decay of  ${}^7\text{Be}$  implanted in Ta, the energy difference between the centroids of the  $K$ -GS and  $L$ -GS peaks in the resulting  ${}^7\text{Li}$  recoil spectrum is predicted to be approximately 6 eV lower than the reference binding energy [21], based on our hypothesis [Eq. (1)]. This result is consistent with the measured energy difference of  $(49.27 \pm 0.06)$  eV [6].

According to Table III, the calculated chemical shifts of the  $1s$  line of  ${}^7\text{Li}$  implanted in different media range from approximately 0 to 2 eV. Therefore, no significant shift in the  ${}^7\text{Li}$   $K$ -GS peak is expected based on these calculations. However, we believe that the  $K$ -GS peak of  ${}^7\text{Li}$  would be shifted down in all those media compared to the HgTe medium, due to their higher Fermi energies relative to HgTe and the difference between the  $K$ -GS and  $L$ -GS peaks would be reduced similar to that observed for the Ta medium. However, we have not tabulated the shift of the  $K$ -GS peak of  ${}^7\text{Li}$  in all these cases because of the difficulty in precisely determining the difference in Fermi energies using the density functional theory code.

The recoil energy spectrum of  ${}^{163}\text{Dy}$  following the electron capture decay of  ${}^{163}\text{Ho}$  implanted in gold was measured [1] and the observed  $3s$ ,  $4s$ ,  $5s$  ground state peaks were found to be shifted downwards by (6–10) eV compared to their measured binding energies with respect to the corresponding Fermi energies. The shift was attributed to the interaction of the additional  $4f$  electron and the condensed matter effect

[23]. We believe that the relaxation of the Auger electron to the Fermi energy of the host gold medium could lower the energies of the  $3s$ ,  $4s$  peaks in the recoil spectrum, consistent with our explanation for the downward shift of the  $K$ -GS peak in the  ${}^7\text{Li}$  recoil spectrum, when  ${}^7\text{Be}$  was implanted in Ta. Our hypothesis could be tested by implanting  ${}^{163}\text{Ho}$  in HgTe and observing the recoil spectrum of  ${}^{163}\text{Dy}$ . If our hypothesis is correct, no significant shifts of  $3s$ ,  $4s$  peaks should be observed in comparison to their binding energies for the implantation of  ${}^{163}\text{Ho}$  in HgTe.

#### IV. CONCLUSIONS

In summary, the increased ( $L/K$ ) ratio of  ${}^7\text{Be}$  implanted in the tantalum lattice compared to that implanted in mercury telluride lattice has been understood quantitatively using *ab initio* density functional WIEN2K code. The calculations compute the  $1s$  and  $2s$  electron densities at the  ${}^7\text{Be}$  nucleus and naturally include all the lattice effects. We have determined ( $L/K$ ) ratios of  ${}^7\text{Be}$  decaying in different media with respect to the experimentally measured ( $L/K$ ) ratio of  ${}^7\text{Be}$  in mercury telluride and tabulate our predictions (Table II) for several untested cases.

We can explain the observed small chemical shift of the oxygen  $1s$  line ( $\approx 1$  eV) between the  $\text{EuCoO}_3$  and  $\text{Sr}_2\text{CoO}_3\text{Cl}$  lattices using the *ab initio* density functional WIEN2K code and predict the expected chemical shifts of the  $1s$  line of lithium atoms implanted in various media relative to the lithium metal. From our density functional calculations, the chemical shift of the  $1s$  state of  ${}^7\text{Li}$  implanted in a large mercury telluride lattice (lattice constant = 6.462 Å) relative to implantation in a small tantalum lattice (lattice constant = 3.306 Å) has been found to be  $\approx -0.8$  eV, implying that the  ${}^7\text{Li}$   $K$ -GS peak would appear at 0.8 eV higher energy when lithium is implanted in Ta compared to when it is implanted in HgTe. We conjecture that the observed large downward shift of the  $K$ -GS peak following the decay of  ${}^7\text{Be}$  in Ta versus HgTe might be due to the substantial difference between the Fermi energies of tantalum and mercury telluride lattices. This result also elucidates the observed reduced energy difference between the centroids of  $K$ -GS and  $L$ -GS peaks for the decay of  ${}^7\text{Be}$  in tantalum, as the position of the  $L$ -GS peak remains almost unchanged, irrespective of the host medium. The observed downward shift of  $3s$ ,  $4s$  peaks in the recoil spectrum of  ${}^{163}\text{Dy}$  [1] compared to their binding energies, along with our predictions regarding the reduction of such a shift in the HgTe medium, offers another potential testing ground for our hypothesis.

#### ACKNOWLEDGMENTS

A.R. acknowledges financial assistance from Science and Engineering Research Board, Government of India, Grant No. CRG/2020/003237. We acknowledge useful discussions with Dr. Y. Nohara.

[1] L. Gastaldo, K. Blaum, K. Chrysalidis, T. Day Goodacre, A. Domula, M. Door, H. Dorrer, Ch. E. Düllmann, K.

Eberhardt, S. Eliseev *et al.*, *Eur. Phys. J. Spec. Top.* **226**, 1623 (2017).

- [2] S. Friedrich, G. B. Kim, C. Bray, R. Cantor, J. Dilling, S. Fretwell, J. A. Hall, A. Lennarz, V. Lordi, P. Machule *et al.*, *Phys. Rev. Lett.* **126**, 021803 (2021).
- [3] C. Velte, F. Ahrens, A. Barth, K. Blaum, M. Braß, M. Door, H. Dorrer, Ch. E. Düllmann, S. Eliseev, C. Enss *et al.*, *Eur. Phys. J. C* **79**, 1026 (2019).
- [4] E. G. Adelberger, S. M. Austin, J. N. Bahcal, A. B. Balantekin, G. Bogaert, L. S. Brown, L. Buchmann, F. E. Cecil, A. E. Champagne, L. de Braekeleer *et al.*, *Rev. Mod. Phys.* **70**, 1265 (1998).
- [5] P. Das and A. Ray, *Phys. Rev. C* **71**, 025801 (2005).
- [6] S. Fretwell, K. G. Leach, C. Bray, G. B. Kim, J. Dilling, A. Lennarz *et al.*, *Phys. Rev. Lett.* **125**, 032701 (2020).
- [7] P. A. Voytas, C. Ternovan, M. Galeazzi, D. McCammon, J. J. Kolata, P. Santi *et al.*, *Phys. Rev. Lett.* **88**, 012501 (2001).
- [8] <https://www.nndc.bnl.gov/>.
- [9] A. Samanta, S. Friedrich, Kyle G. Leach, and V. Lordi, *Phys. Rev. Appl.* **19**, 014032 (2023).
- [10] A. Ray, P. Das, S. K. Saha, S. K. Das, and A. Mookerjee, *Phys. Rev. C* **66**, 012501(R) (2002).
- [11] J. N. Bahcall, *Phys. Rev.* **128**, 1297 (1962).
- [12] W. Bambynek, H. Behrens, M. H. Chen, B. Crasemann, M. L. Fitzpatrick, K. W. D. Ledingham *et al.*, *Rev. Mod. Phys.* **49**, 77 (1977).
- [13] P. Blaha, K. Schwarz, F. Tran, R. Laskowski, G. K. H. Madsen, and L. D. Marks, *J. Chem. Phys.* **152**, 074101 (2020).
- [14] Z. Hu, H. Wu, M. W. Haverkort, H. H. Hsieh, H.-J. Lin, T. Lorenz, J. Baier, A. Reichl, I. Bonn, C. Felser, A. Tanaka, C. T. Chen, and L. H. Tjeng, *Phys. Rev. Lett.* **92**, 207402 (2004).
- [15] [www.webelement.com](http://www.webelement.com).
- [16] *CRC Handbook of Chemistry and Physics*, edited by D. R. Lide (CRC Press, Boca Raton, FL, 1994).
- [17] O. Pekinchak, L. Vasylechko, V. Berezovets, and Y. Prots, *Solid State Phenom.* **230**, 31 (2015).
- [18] C. S. Knee, D. J. Price, M. R. Lees, and M. T. Weller, *Phys. Rev. B* **68**, 174407 (2003).
- [19] A. Ray, P. Das, A. K. Sikdar, S. Pathak, M. Lozano-Espinosa N. Aquino, and A. N. Artemyev, *Eur. Phys. J. D* **75**, 140 (2021).
- [20] J. N. Bahcall, *Phys. Rev. Lett.* **9**, 500 (1962).
- [21] J. A. Bearden and A. F. Burr, *Rev. Mod. Phys.* **39**, 125 (1967).
- [22] O. K. Andersen, Z. Pawłowska, and O. Jepsen, *Phys. Rev. B* **34**, 5253 (1986).
- [23] P. C. -O. Ranitzsch, C. Hassel, M. Wegner, S. Kempf, A. Fleischmann, C. Enss, L. Gastaldo, A. Herlert, and K. Johnston, [arXiv:1409.0071](https://arxiv.org/abs/1409.0071).